

PFC/JA-94-33

## Overview of Recent Results from Alcator C-Mod<sup>†</sup>

Miklos Porkolab  
and the Alcator Group<sup>‡</sup>

Plasma Fusion Center  
and Department of Physics  
Massachusetts Institute of Technology  
Cambridge, MA 02139

October 1994

Presented at the Fifteenth International Conference on Plasma Physics and Controlled Nuclear Fusion Research, Seville, Spain, 26 September – 01 October 1994, IAEA-CN-60/A-1-II-2. To be published in the Proceedings of the Conference.

<sup>†</sup> This work was supported by the U.S. Department of Energy Contract No. DE-AC02-78ET51013.

<sup>‡</sup> M. Porkolab, R. Boivin, F. Bombarda<sup>1</sup>, P. Bonoli, C. Christensen, D. Garnier, S. Fairfax, C. Fiore, J. Goetz, S. Golovato, M. Graf, R. Granetz, M. Greenwald, D. Gwinn, S. Horne, T. Hsu, A. Hubbard, I. Hutchinson, J. Irby, D. Jablonski, C. Kurz, B. LaBombard, B. Lipschultz, T. Luke, E. Marmor, M. May<sup>2</sup>, A. Mazurenko, G. McCracken, R. Nachtrieb, A. Niemczewski, P. O'Shea, J. Reardon, J. Rice, J. Schachter, J. Snipes, J. Sorci, P. Stek, Y. Takase, J. Terry, G. Tinios, J. Urbahn, Y. Wang, R. Watterson, B. Welch<sup>3</sup>, S. Wolfe

---

<sup>1</sup> *ENEA Frascati, Via Enrico Fermi, 27, 00044 Frascati (Rome), Italy*

<sup>2</sup> *The John Hopkins University, Department of Physics, Baltimore, MD*

<sup>3</sup> *University of Maryland, College Park, MD*

# OVERVIEW OF RECENT RESULTS FROM ALCATOR C-MOD

## ABSTRACT

Alcator C-Mod, a compact high magnetic field, high density, diverted and shaped tokamak has been operating at MIT since May, 1993. Unique ITER relevant features of the machine include a thick conducting vacuum vessel, all molybdenum plasma facing components, and a closed divertor geometry. An overview of recent results is presented, with particular emphasis on MHD studies including halo currents, confinement studies with ohmic and ICRF heating, and divertor research with emphasis on dissipative divertor operations. Key results presented include quantitative studies of halo current formation (up to 20% of  $I_p$ ), effective ICRF heating (up to 2 MW) with well controlled metallic impurity generation, demonstration of dissipative divertor operation (both radiative and detached), and extension of the H-mode threshold database by more than an order of magnitude ( $\bar{n}_e B_T \sim 10^{21} T/m^3$ ,  $P/S \sim 0.35 \text{ MW/m}^2$ ).

## 1. INTRODUCTION

Alcator C-Mod is a high magnetic field, high current density, ICRF heated compact tokamak with flexible divertor and shaping capabilities (see Fig. 1). Its unique features include a thick conducting vacuum vessel, all molybdenum plasma facing components, and a closed divertor geometry, all of which may be prototypical of future devices including ITER and DEMO [1]. The design parameters are:  $B_T \lesssim 9 \text{ T}$ ,  $I_p \lesssim 3 \text{ MA}$ ,  $\kappa \lesssim 1.8$ ,  $R = 0.67 \text{ m}$ ,  $a = 0.22 \text{ m}$ ,  $t_{pulse} \sim t_{L/R}$ , and  $P_{ICRF} \simeq 8 \text{ MW}$ . With noninductive current drive added in the future, pulse lengths up to 7 sec (or  $5t_{skin}$  at  $T_e \lesssim 5 \text{ keV}$ ) are feasible at 5 Tesla. With the full ICRF power the plasma surface power density is in the range  $0.5\text{-}1.0 \text{ MW/m}^2$ , the heat flux in the SOL is  $q_{||} \simeq 0.5 - 1.0 \text{ GW/m}^2$ , and the RF power density on the antenna surface is  $P_{ICRF}/A \sim 10 \text{ MW/m}^2$ , which are comparable to those required for ITER and DEMO. A 20 shot deuterium pellet injector (with pellet speeds up to 1300 m/sec) is available for fueling and density profile control. The injector is configured to fire up to 5 pellets each of 4 different sizes. The present ICRF power capability is 4.0 MW at a frequency of 80 MHz, which is suitable for minority heating in deuterium majority plasmas at  $B_0 = 5.3 \text{ T}$  ( $\text{H}^+$  minority) and  $B_0 = 7.9 \text{ T}$  ( $^3\text{He}^{++}$  minority). This power will be increased to 8 MW in 1996 by adding 4 MW of 40–80 MHz variable-frequency power.

Alcator C-Mod commenced operation in May, 1993 and to date the following plasma parameters were achieved:  $B_T \leq 5.3 \text{ T}$ ,  $I_p \leq 1.05 \text{ MA}$ ,  $\kappa \leq 1.7$ ,  $t_{pulse} \leq 1.3 \text{ sec}$ ,  $n_{e0} \leq 1 \times 10^{21} \text{ m}^{-3}$ ,  $T_i \leq T_e \leq 3.2 \text{ keV}$ ,  $P_{RF} \leq 1.8 \text{ MW}$ . Some of the key research topics investigated during the past year and discussed in this paper include the following:

(a) effective MHD control, including studies of disruptions, vertical stability and halo currents; (b) demonstration of effective ICRF heating; (c) divertor research, with particular emphasis on a quantitative study of dissipative divertor operation with a closed divertor; (d) transport studies in a unique parameter regime.

## 2. MHD PHENOMENA AND HALO CURRENTS

In the MHD area, much effort has been devoted to investigating plasma control, disruptions, ELMs, and pellet-induced snakes. Disruptions in Alcator C-Mod tend to be rather fast, with peak values of  $dI_p/dt$  up to 1.0 MA/ms, with  $dI_p/dt$  roughly proportional to  $I_p$ . Nearly all disruptions are either caused by, or result in fast vertical displacement of the plasma, leading to substantial poloidal “halo” currents in the plasma edge and conducting structures. Given the relatively high toroidal magnetic field, the halo currents flowing in both the inboard wall of the vacuum vessel and the outer divertor modules result in substantial  $j \times B$  forces on the first wall and plasma facing components. In order to measure the direction and magnitude of the halo currents and to examine the scaling with plasma current  $I_p$ ,  $dI_p/dt$ , and vertical velocity, several diagnostics have been installed on the inboard wall, the outer divertor modules, and outboard limiters. We find that the polarity of halo currents flowing in the vessel wall is such that the resulting force on the inboard wall is radially inward, and that the magnitude of the current scales at least linearly with  $I_p$ . For disruptions with  $I_p \leq 1$  MA, the observed halo currents can be as much as 20% of  $I_p$ .

To study vertical stability, in a series of discharges the vertical position feedback control was temporarily turned off while the plasma was vertically unstable. The vertical position was fitted to an exponential and compared to growth rates calculated using a perturbed equilibrium model [2]. To study the closed loop response, we inserted steps into the programmed Z-position and observed how the plasma relaxed to a new equilibrium after each jump. Agreement with the models for both closed-loop and open-loop response was within a factor of two.

## 3. ICRF HEATING AND IMPURITY RADIATION

ICRF coupling and heating experiments were carried out with both a movable single-strap (monopole) antenna and a fixed two-strap (out of phase operation) dipole antenna [3]. Both antennas are coated with TiC/N. Up to 1.8 MW of power has been coupled into the plasma at an rf power density of  $\sim 10$  MW/m<sup>2</sup> on the antenna surface. A second dipole antenna, with a Boron-Carbide (B<sub>4</sub>C) coated Faraday shield, has been installed in an adjacent port, and will be powered with a second 2 MW transmitter at 80 MHz during the next experimental campaign. Typical antenna loading observed is in the range of 3–25

ohms, depending on plasma density and antenna-separatrix spacing with the lowest loading observed during ELM-free H-mode periods, and the highest loading occurring at high densities in limited discharges. A typical ICRF heated 0.7 MA discharge time-sequence using the dipole antenna is shown in Fig. 2. As shown in Figs. 2 and 3, significant plasma heating is observed during H minority ( $\sim 2\text{-}10\%$  concentration) heating at 5.3 T in deuterium majority plasmas. The range of plasma parameters covered in the ICRF heating experiments is  $0.4 \leq I_p$  (MA)  $\leq 1.0$ ,  $0.5 \leq \bar{n}_e(10^{20}\text{m}^{-3}) \leq 2.0$ , with  $\Delta T_i \leq 1.3$  keV,  $\Delta T_e \leq 1.4$  keV.

For ohmic plasmas with  $\bar{n}_e$  above  $1.5 \times 10^{20}\text{m}^{-3}$ ,  $Z_{eff}$  is  $< 1.3$  (measured by visible Bremsstrahlung emission), and the fraction of the input power radiated is  $\sim 50\%$  (measured bolometrically). Spectroscopic measurements show the major low Z impurity to be carbon, found in concentrations of  $< 1\%$ . The molybdenum density, the first wall and divertor plate material, decreases for  $\bar{n}_e > 1.5 \times 10^{20}\text{m}^{-3}$  to concentrations of  $< 0.01\%$ . When the plasma configuration changes from limited (on the inner wall) to diverted, the density of molybdenum typically drops, consistent with the observation that the molybdenum influx comes predominantly from the inner wall. The influx from the divertor target plates is usually negligible [4].

One of the critical issues to be answered by these experiments is the production of metallic (molybdenum) impurities and radiative losses during ICRF heating. As evidenced in Fig. 4, when heating with the monopole antenna, the integrated radiated power from inside the last closed flux surface (LCFS) increases linearly with  $P_{in}$ , and  $P_{rad}/P_{in} \sim 75\%$  for  $P_{RF} > 0.5$  MW. The increase in  $P_{rad}$  is due almost entirely to the increase in Mo influx observed in these cases. Using the dipole antenna, the radiated power fraction is substantially reduced, remaining at  $\sim 50\%$  up to the highest power injected to date. For a given RF power, comparisons of the relative Mo influxes using the monopole and dipole antennas show a factor of  $\sim 6$  decrease for the dipole case. In all cases, bolometric profiles show that the radiation is peaked toward the edge of the plasma. Because of systematically improved heating in the dipole cases, the location of the peak is very close to the edge, consistent with the fact that Mo is an efficient radiator for  $T_e \sim 600$  eV. With the dipole antenna,  $Z_{eff}$  increases by  $\sim 0.2$  at the highest ICRF powers. Observed increases in the carbon and Mo concentrations account for a majority of this  $Z_{eff}$  change. As seen in the figure, the fraction of the input power which is radiated inside of the LCFS does not increase during auxiliary heating with the dipole antenna, as compared to the pure ohmic heating phase. These results indicate the potential for increased ICRF power injection and heating without serious impurity problems in the next phase of operations.

## 4. DIVERTOR PHYSICS RESULTS

Alcator C-Mod operates with an inclined molybdenum divertor plate and a closed divertor geometry. With this configuration two forms of dissipative divertor operation are achieved. The first is the high-recycling divertor where the density at the plate ( $< 6 \times 10^{20} \text{m}^{-3}$ ) can be as high as 5–10 times that at the midplane. The plasma pressure is approximately constant along a flux surface with power flow along a flux surface well-described by conductive (as opposed to sheath-limited) flow [5]. The temperature profile at the outer divertor plate is inverted (see Fig. 5), namely  $T_e$  increases as a function of distance from the separatrix in the inclined plate region [6]. This profile may be related to the inclined plate geometry which directs recycling neutrals towards the separatrix, increasing  $n_e$  there. With the above divertor conditions the volumetric power losses in the divertor region are often 40% of the input power (70-80% of the power flowing into the SOL); the dominant losses are from carbon radiation and charge-exchange [7]. The retention of gaseous recycling impurities has also been investigated; for example, Ne and Ar are all well confined in the divertor (fewer than 2% of the injected particles are found inside the separatrix) [8].

In the second (dissipative) divertor operational mode, the plasma becomes detached from both the inner and outer divertor plates. The most important characteristics are the following [6]: the pressure and density decrease at the plate (see Fig. 5) over a limited region around the separatrix which appears to correlate with the extent of the inclined plate region (see Fig.1 Ref. [8]). The transition occurs abruptly and the divertor radiation shifts from the divertor to the x-point region. Impurity and hydrogen neutrals penetrate more easily into the central plasma, leading to increased density and impurity concentration. Prior to the rapid divertor detachment transition, the plasma pressure decreases gradually in the inclined plate region of the outer divertor plate. Since  $T_{e,plate}$  is always  $\sim 5$  eV prior to detachment, we believe that the power flowing to the divertor plate is an important factor in determining whether divertor detachment occurs. After detachment,  $T_{e,plate}$  decreases to the 1–3 eV range. The critical electron density for detachment is linearly dependent on  $P_{in}$ . In cases where a central plasma with a detached divertor is heated with RF power the detachment process can be reversed and reattachment is observed (Fig. 5). This is due to the increased power into the SOL and consequent higher  $T_e$  at the plate.

## 5. CONFINEMENT AND TRANSPORT

The confinement results achieved to date in C-Mod are summarized by Greenwald et al. in a companion paper at this Conference [9]. In contrast to the Alcator-C results [10] we find that in C-Mod the confinement can be fit with ITER89-P L-mode scaling [11] for both ohmic and ICRF heated plasmas (see Fig. 6). The minority ion tail stored energy is

estimated to be 10–15 kJ at the highest power level [9]. The confinement in both ohmic and ICRF heated plasmas shows no clear dependence on density, but it improves with plasma current ( $\tau_E \propto I_p$ ) and degrades as  $P_{tot}^{-1/2}$ . In general, the confinement in ohmic and ICRF heated plasmas are distinguishable only by the relative values of the total input power.

H-modes have been achieved in Alcator C-Mod with ohmic heating alone and with ICRF power added in lower single null diverted, as well as inner wall limited discharges. ELM-free ohmic H-modes were achieved by ramping down the toroidal field to about 3 T and ELMy ohmic H-modes have been achieved at constant toroidal fields up to 5.25 T and  $\bar{n}_e < 1.4 \times 10^{20} \text{m}^{-3}$  [12]. Both ELMy and ELM-free ICRF H-modes have been obtained with constant toroidal field up to 5.37 T and  $\bar{n}_e < 1.8 \times 10^{20} \text{m}^{-3}$  with the ion grad-B drift toward the divertor. By comparing ohmic and ICRF ELMy H-modes, there appears to be an inverse scaling of the ELM frequency with input power, consistent with the ELMs being of Type III. A typical ICRF H-mode time sequence is shown in Fig. 7. The net RF power decreases by as much as 40%, but the stored energy remains constant. Meanwhile, the density rises significantly until the power is no longer sufficient to maintain the H-mode. The plasma returns to the L-mode phase, and the whole cycle repeats  $\sim 20$  ms later.

One of the important results of C-Mod is the extension of the H-mode power-threshold database to a surface power density,  $P/S$  of  $0.35 \text{ MW/m}^2$ , and the  $\bar{n}_e B_T$  product to 9.5 (in units of  $10^{20} \text{m}^{-3}$  and Tesla). Figure 8 depicts the C-Mod H-mode threshold results for both ohmically and ICRF heated plasmas. Also shown in the figure are data published from DIII-D [13] and ASDEX-U [14]. We see that the previously established threshold scaling, namely  $P/S \propto \bar{n}_e B_T$ , is followed with a proportionality constant of  $\sim 0.044$  in the above units. Although the ELMy H-mode thresholds can be as much as 50% below the above scaling, their confinement improvement is limited to  $< 50\%$  increase above the L-mode confinement (in contrast to the ELM-free cases where  $\tau_E$  improvements of a factor of two or more are observed). It should be noted that no special wall-conditioning technique (other than the standard low-power electron cyclotron discharge cleaning) was necessary to achieve H-mode confinement in the metal-walled C-Mod chamber. However, preliminary results suggest that wall coating following Li pellet injection may result in reduced H-mode threshold.

## 6. CONCLUSIONS

Alcator C-Mod has been operating successfully with an all-metallic plasma facing environment with ITER relevant plasma parameters and power flux. In the area of plasma operation, disruption rates in excess of 1 MA/ms, and halo currents of up to  $0.2 I_p$  have

been observed. Effective ICRF heating has been demonstrated with a dipole antenna at densities up to  $\bar{n}_e = 2 \times 10^{20} \text{m}^{-3}$  with no adverse metallic impurity injection. The confinement scaling is in agreement with ITER89-P L-mode scaling, for both ohmic and ICRF heated plasmas. H-mode confinement has been achieved, and for ELM-free H-modes the threshold power follows the previously established scaling, extending the regime by an order of magnitude to ITER-relevant values. Effective dissipative divertor operation has been demonstrated with a closed divertor with molybdenum tiles, including both a high-recycling mode and a detached-plasma type of operation.

### ACKNOWLEDGEMENT

We thank the C-Mod engineering and technical staff for their important contributions to this research.

### REFERENCES

- [1] HUTCHINSON, I.H., et al., Physics of Plasmas, **1** (1994) 1511.
- [2] HUMPHREYS, D.A., et al., Fusion Technology, **23** (1993) 167.
- [3] GOLOVATO, S., et al., Proc. 20th Eur. Conf. on Controlled Fusion and Plasma Physics, Montpellier, France 1994 (to be published).
- [4] KURZ, C. et al., Proc. 11th Int. Conf. on Plasma-Surface Interactions, Mito, Japan, 1994 (to be published).
- [5] LaBOMBARD, B., et al., Proc. 11th Int. Conf. on Plasma-Surface Interactions, Mito, Japan, 1994 (to be published).
- [6] HUTCHINSON, I.H., et al., Proc. 20th Eur. Conf. on Controlled Fusion and Plasma Physics, Montpellier, France 1994 (to be published).
- [7] LIPSCHULTZ, B., et al., Proc. 11th Int. Conf. on Plasma-Surface Interactions, Mito, Japan, 1994 (to be published).
- [8] TERRY, J.L., et al., IAEA-CN-60/A-4-I-6, at this Conference.
- [9] GREENWALD, M., et al., IAEA-CN-60/82/4-P-2, at this Conference.
- [10] PARKER, R., et al., Nucl. Fusion **25** (1985) 9.
- [11] YUSHMANOV, P.N., et al., Proc. 20th Eur. Conf. on Controlled Fusion and Plasma Physics, Montpellier, France 1994 (to be published).
- [12] SNIPES, J., et al., Proc. 20th Eur. Conf. on Controlled Fusion and Plasma Physics, Montpellier, France 1994 (to be published).

[13] OSBORNE, T.H., et al., Nucl. Fus. **30**, (1990) 10.

[14] RYTER, F. et al., 20th EPS Conf. on Controlled Fusion and Plasma Physics, Proc. **17C** (1993) I-23.



## FIGURE CAPTIONS

Fig. 1: Cross sectional view of C-Mod detailing a typical plasma shape, equilibrium field coils, open (upper) and closed (lower) divertor geometry, and the two-strap ICRF antenna.

Fig. 2: Typical time evolution of plasma parameters during ICRF injection at  $B_T = 5.3$  T,  $I_p = 0.7$  MA.  $\bar{n}_e$  is measured by a 10-chord CO<sub>2</sub> interferometer,  $T_e$  by electron cyclotron emission,  $T_i$  by neutron emission, and the stored energy by EFIT magnetic equilibrium reconstruction.

Fig. 3: Typical values of  $\Delta T_i(0)$  versus  $P_{RF}/\bar{n}_e$  during ICRF heating.

Fig. 4: Radiated power as a function of total input power for ohmic and ICRF heated plasmas. The radiated power is calculated from the radiation profiles measured with the tangentially viewing midplane bolometer array, integrated from the center of the plasma out to the last closed flux surface.

Fig. 5:  $n_e$  and  $T_e$  at the outer divertor plate are plotted vs. the corresponding midplane distance outside the separatrix. Open symbols correspond to detached divertor plasma before RF heating. Closed symbols correspond to reattached divertor plasma during RF heating.

Fig. 6: Plasma thermal stored energy versus total input power for various ranges of  $I_p$ . The solid lines represent the expected values based on ITER89-P scaling at 0.4, 0.6 and 0.8 MA respectively. Shots included have  $I_p$  within 10% of the nominal value plotted.

Fig. 7: Typical ICRF H-mode time-sequence.

Fig. 8: H-mode threshold data, with DIII-D [13] and ASDEX-UG [14] shown for comparison.

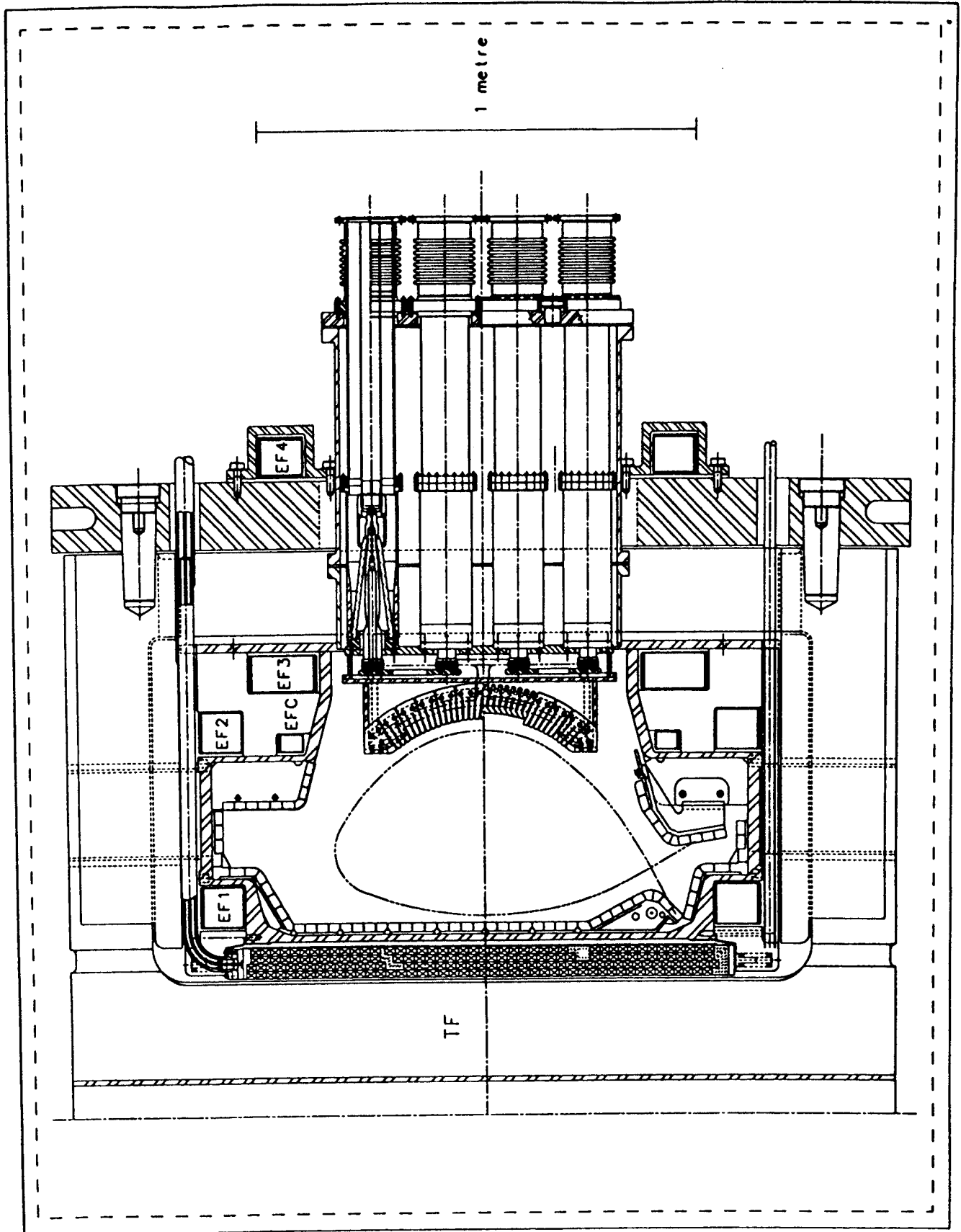


Fig. 1

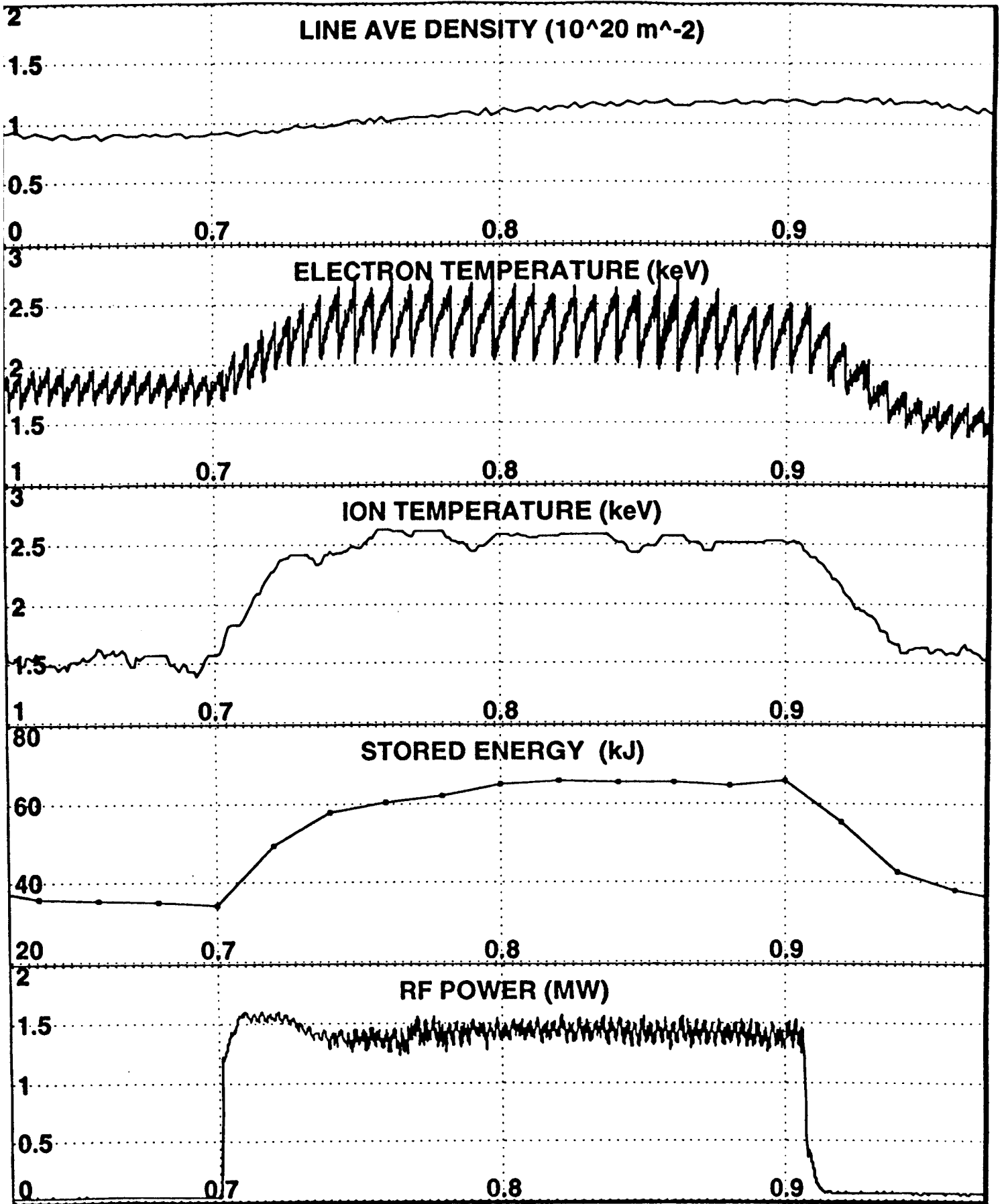


Fig. 2

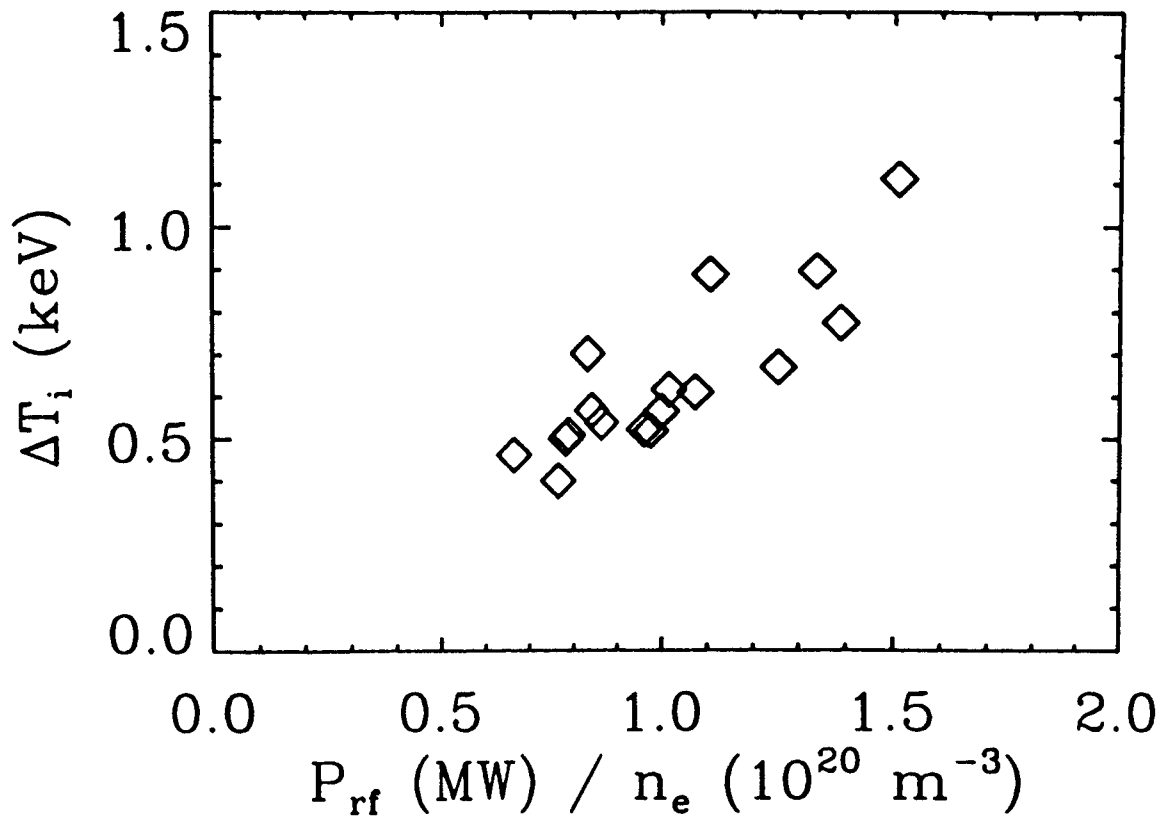


Fig. 3

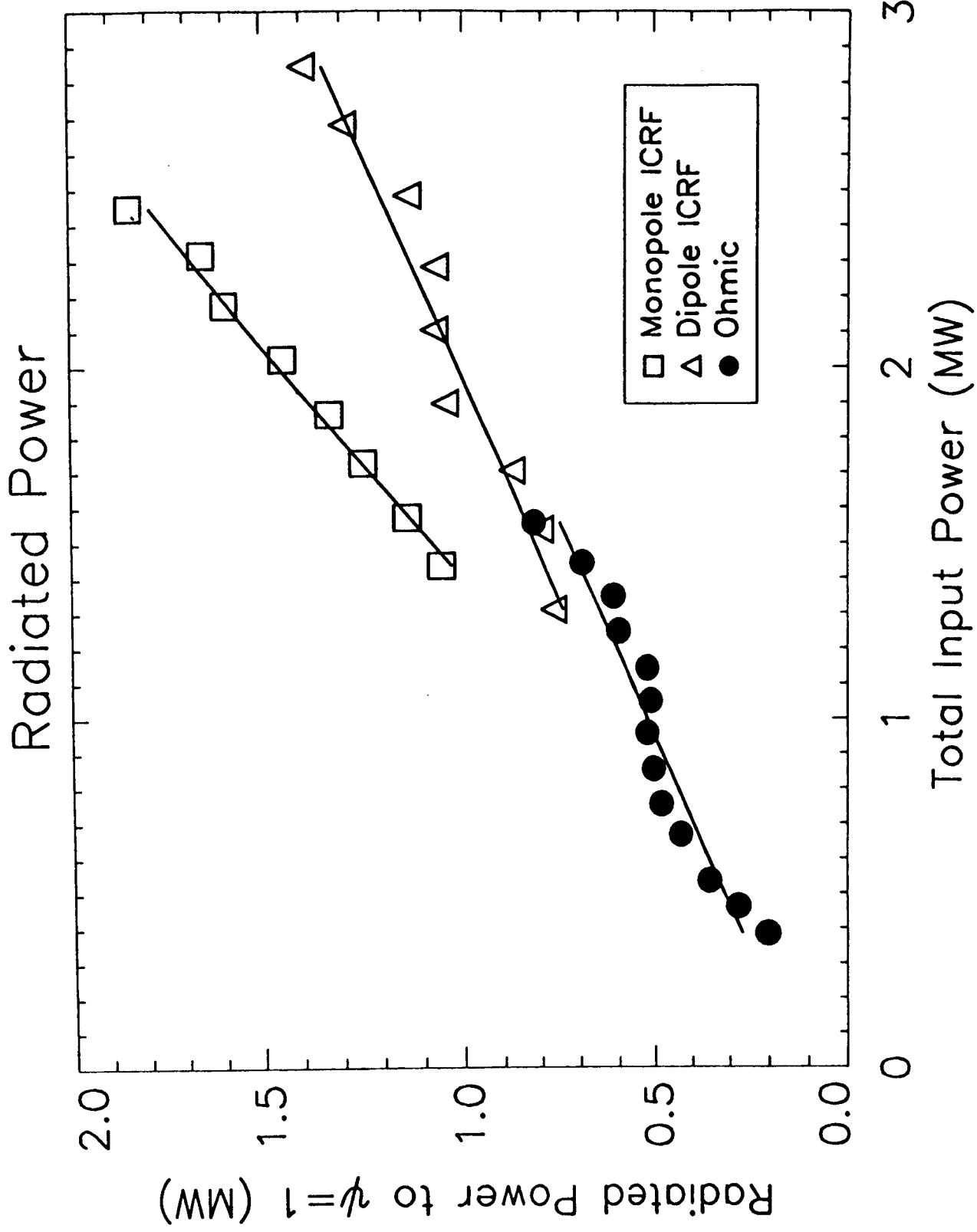


FIG. 4

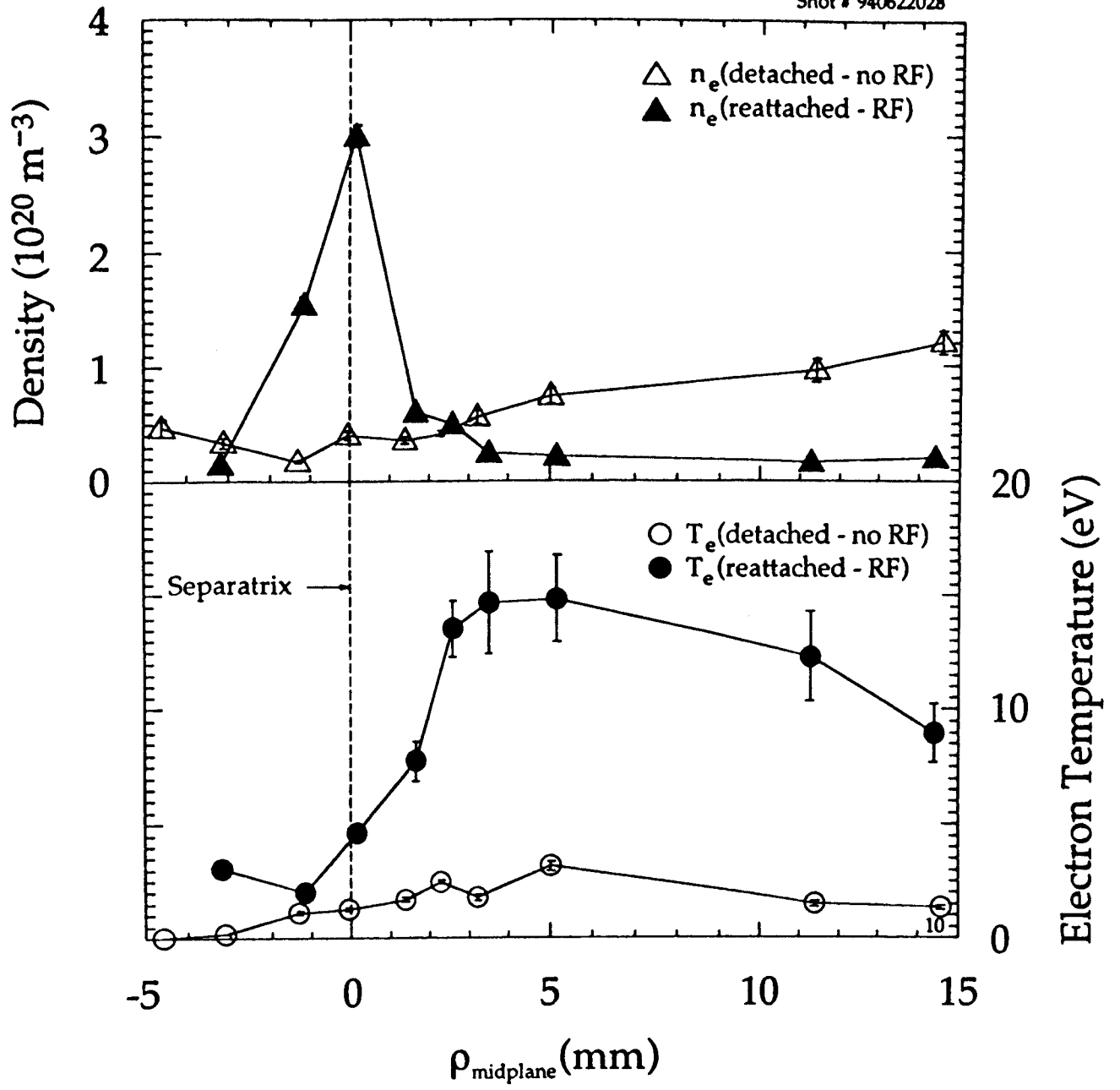


Fig. 5

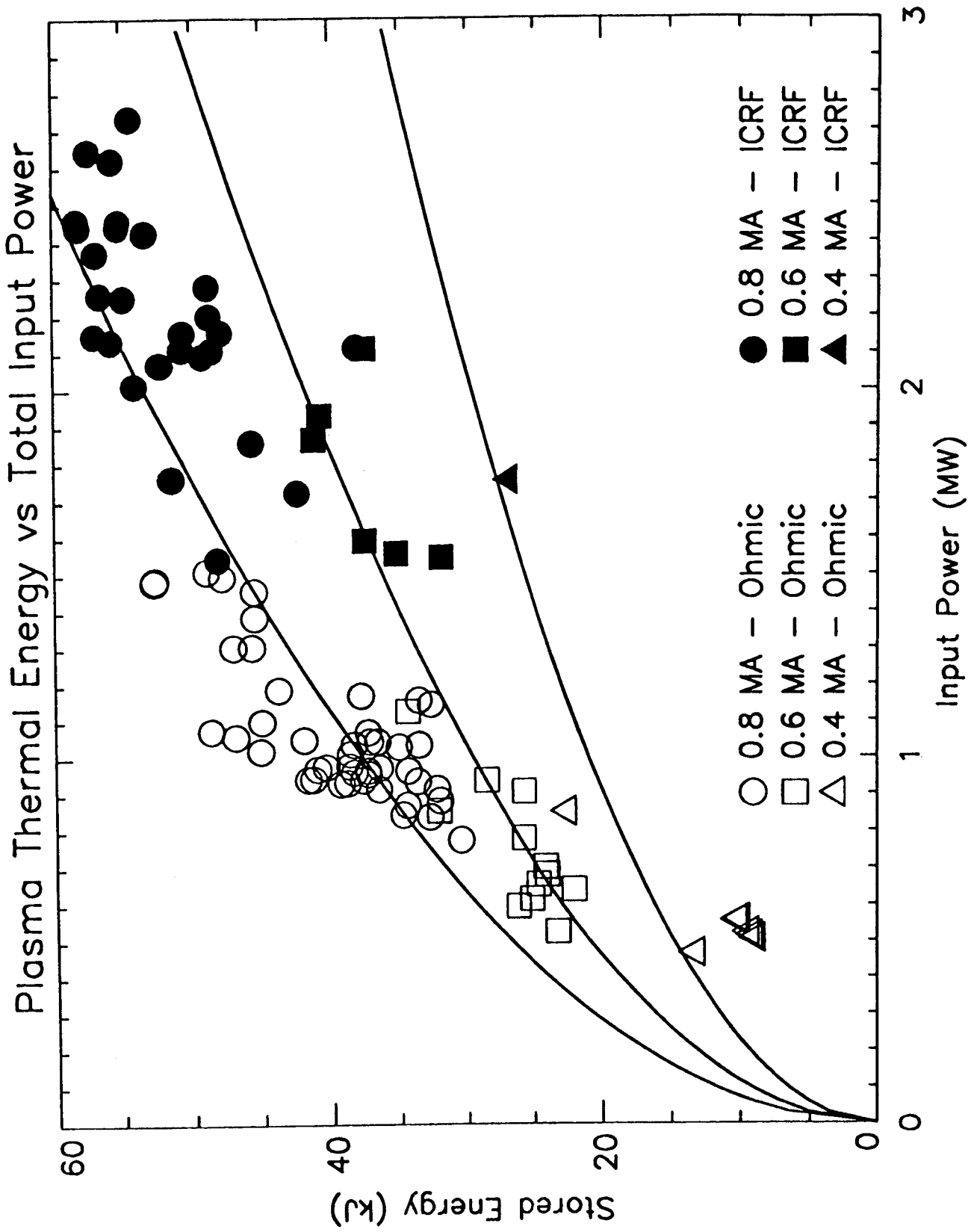


Fig. 6

SHOT 940608005

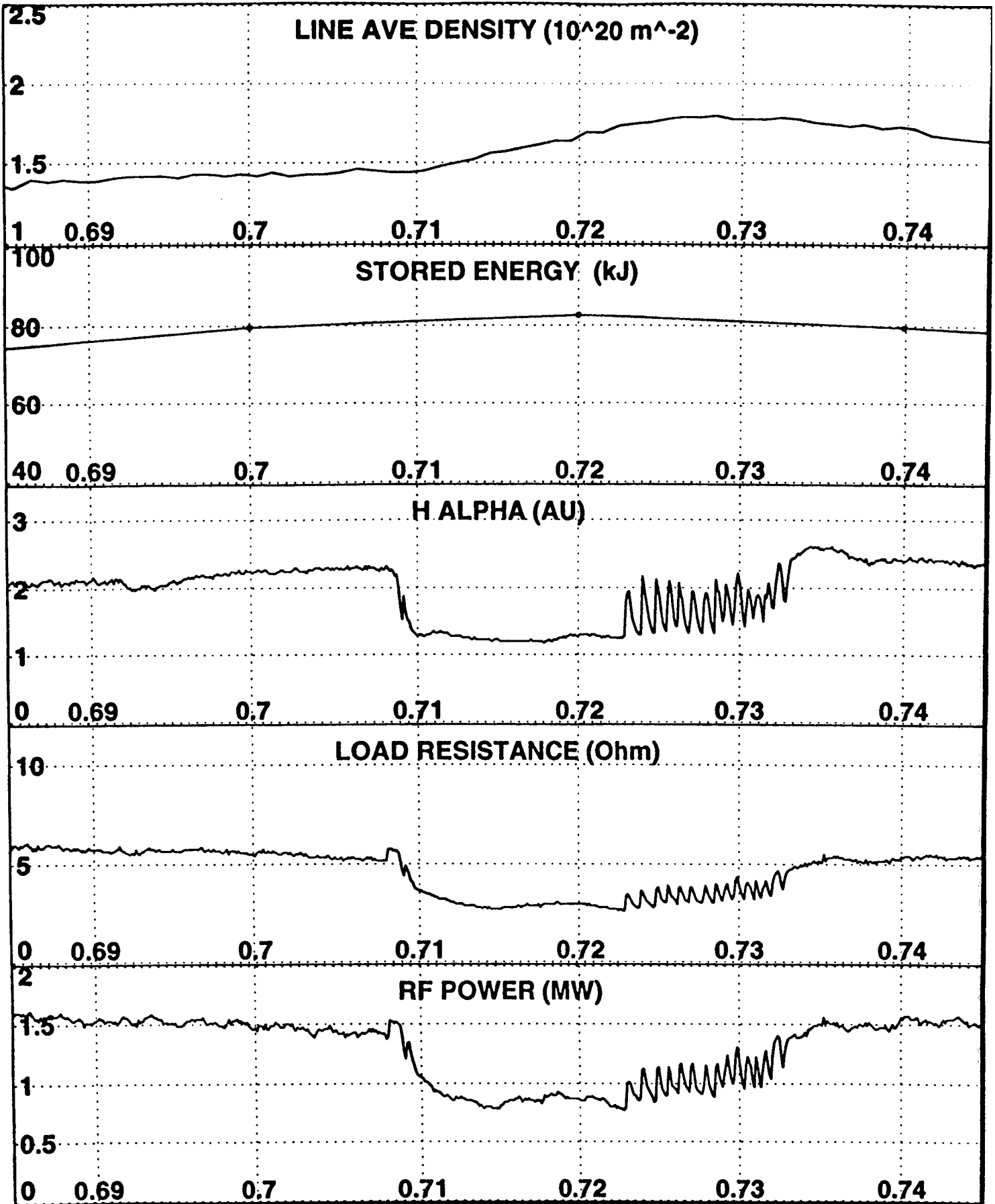


Fig. 7



# ICRH and Ohmic H-Mode Threshold

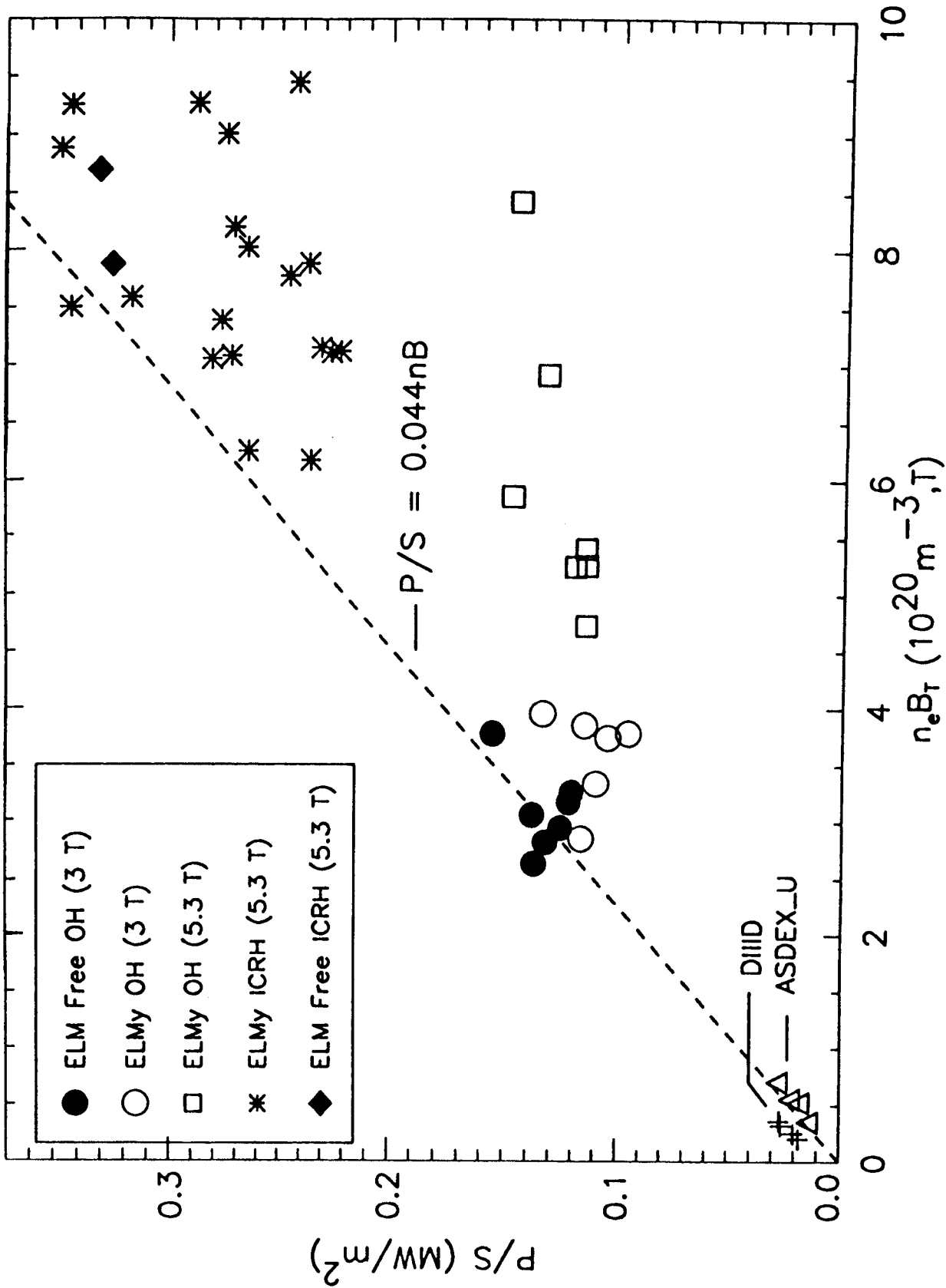


Fig. 8